Journal of Manufacturing Processes 126 (2024) 348–357

Contents lists available at ScienceDirect

Journal of Manufacturing Processes

journal homepage: www.elsevier.com/locate/manpro

Optimization of the layer quality by TiC nanoparticles in the ultrasonic excited recoating process with non-spreadable AlSi10Mg matrix B4C particle-powder composites for powder bed based additive manufacturing

Victor Lubkowitz *, Kai Drechsel, Volker Schulze, Frederik Zanger

wbk Institute of Production Science, Karlsruhe Institute of Technology (KIT), Kaiserstr, 12, 76131 Karlsruhe, Germany

ARTICLE INFO

Keywords:
PBF-LB
Ultrasonic excitation
Recoating
Metal matrix composites
Agglomerating powders

ABSTRACT

High-strength and stiffness materials can further increase the lightweight construction potential of additive manufacturing. One way to achieve this, is to produce particle-reinforced aluminum matrix composites (PAMCs). A significant increase in strength can be achieved with ceramic particles smaller than 6 µm and a volume fraction of 20 to 30 % in other metallurgical processes. Due to the larger interparticle forces compared to the gravitational force, such powder mixtures are not flowable and cannot be recoated in PBF-LB with static recoaters like rubber lips and metal blades. Two approaches were compared to solve this problem. Firstly, the new broadband ultrasonic excitation of the recoater metal combs and secondly, flow enhancing with nanoparticles. The influence of the approaches was investigated by image analysis of the recoated layers for defects in an SLM 280 HL 1.0. Broadband vibration enables reliable recoating of AlSi10Mg powders mixed with up to 20 vol% 6 µm boron carbide particles without layer defects. Combined with TiC nanoparticle coating, 25 vol% are possible. The solution can securely be operated in build jobs.

1. Introduction

Topology optimization determines the structure-relevant volume of a given design space and loading case, whereby geometries with the lowest possible weight are found [1]. These structures cannot usually be produced by conventional manufacturing processes, but by additive manufacturing, e.g. laser powder bed fusion (PBF-LB) for metallic components. Topology-optimization results depend on the chosen material and its properties. Materials with high stiffness and yield strength are especially preferred for lightweight construction. While a variety of materials are available for conventional production, the availability of powders suitable for the PBF-LB process is limited [2]. The processing of high-strength materials, often used in conventional manufacturing processes with high carbon content in steels [3] or copper precipitates in aluminum (group EN AW7xxx) is especially problematic in PBF-LB [3]. The subject of research is currently modifying the alloy composition to create new high-strength aluminum alloys [4–6] or to enable the processing of high-strength lightweight materials [7]. In these approaches, rare elements are often used to either increase strength or to reduce crack susceptibility. Using rare elements inevitably increase the price of the materials.

An alternative cheap approach is the production of particle-reinforced aluminum matrix composites (PAMCs) to increase the mechanical properties. An increase in stiffness and strength was observed in powder metallurgical production (hot pressing + extrusion) of PAMCs or casting processes. In metallurgical production, fatigue strengths, yield strengths, and elastic moduli increase, when the grain size of SiC reinforcements decrease. The best results were observed at an average particle diameter of 5–6.5 µm. The ideal volume fraction of SiC particles is between 20 and 30 vol% [8].

Currently, the production of metal matrix composites (MMCs) is under investigation in the PBF-LB process. One challenge in the processing of MMC powder feedstocks is the recoating. Usually, spherical powders without fine particles <20 µm are used to ensure recoatability. Spherical powders are used to avoid interlocking of the particles [9–11]. Fine particles are removed because the gravitational force acting on these particles is less than the adhesive forces (Van der Waals forces and the electrostatic forces) between the particles, causing the powder particles to agglomerate [12,13]. Additionally, the specific surface area of the fine particles increases which directly correlates with increasing internal powder friction, resulting in a decrease in flowability [14]. For a good reinforcing effect, fine particles need to be added back in blocky

* Corresponding author.
E-mail address: victor.lubkowitz@kit.edu (V. Lubkowitz).

https://doi.org/10.1016/j.jmapro.2024.07.118
Received 22 November 2023; Received in revised form 3 June 2024; Accepted 24 July 2024
Available online 1 August 2024

shape in large quantities dramatically reducing the feedstock flowability as the particles agglomerate. Most investigations reported difficulties in recoating their MMC feedstocks [15], limiting the maximum vol% of fine ceramic particles [16]. Other researchers used self-built process chambers to study MMCs with a high amount of fine ceramic particles, but do not explain the recoating process in detail [17]. It is assumed that the recoating velocity was significantly reduced to reach a sufficient layer quality [18–20]. However, this reduces the economic efficiency of the process. Others used large reinforcement particles [21], which do not agglomerate.

One option to increase the flowability of powder feedstocks, even with fine particles, is to coat them with ceramic nanoparticles. The presence of nanoparticles increases the distance between the particles reducing the adhesive forces between them [22–25]. Moreover, a greater particle distance reduces capillary forces, resulting in a lower number of liquid bridges [26,27]. Additionally, the nanoparticles act as ball bearings [28]. All effects increase the flowability of powders independent of the selected ceramic material itself. Fulchini et al. [29] investigated the optimum amount of nanoparticles required to improve flowability and determined an ideal particle surface coverage of 20 %. In addition, Gärtner et al. [30] conducted a more detailed study and found that the optimal surface coverage for improved flowability is 25 %. They achieved a significant increase in the fines volume concentration (particles <20 µm) of AlSi10Mg and 316 L to 37 % and 32 % of the total powder raw material, respectively, using nanoparticle coatings that resulted in good flowing powders. The improvement in flowability and the ideal coating of 25 % of the particle surface with TiC nanoparticles were confirmed in our investigations [31]. However, coating was not sufficient to enable defect-free coating of PAMCs. For this reason, a new recoating system approach is needed to recoat non-flowable PAMCs without significantly reducing the recoating velocity.

Vibration excitation is another option to increase the flowability of dry, agglomerating powders. In process engineering, vibration excitation is used in silos, in sieves, for transport or for dosing of dry powders [32–34]. Kollmann et al. [35] found that excitation at 100 Hz can significantly reduce shear stress (a measure of flowability) within TiO2 and CaCO3 particles with an average diameter of 1 µm, leading to a possible reduction of a silo discharge diameter and silo hopper angle. The mechanism of action was described experimentally and mathematically by Teidelt et al. [36]. They proved that the friction coefficient between different materials is reduced with a 45 kHz vibration excitation independent of the excitation direction. An orthogonal excitation causes the friction partner to lose contact for a short time. A longitudinal excitation causes a change in the relative velocity between the friction partners. In both cases, the friction coefficient decreases overall over the course of an excitation period. Dunst et al. [37] have also observed this phenomenon in powder materials. A 20 kHz excitation could fluidize flour as the friction coefficient was reduced. It was also shown that the friction coefficient was reduced more with orthogonal excitation than with longitudinal excitation. Schiochet et al. [38] proved in a discrete element method (DEM) simulation that vibration excitation improves the powder layer quality (increase of powder bed density). However, only a flowable and recoatable PA12 powder was considered, and a real implementation is still missing.

Based on the considerations mentioned above, the aim is to develop a new ultrasonically excited recoating system that allows to process non-flowable agglomerating PAMC powder feedstocks. For this purpose, recoating with broadband ultrasonically energized metal combs is designed and implemented in a SLM280HL 1.0 from Nikon SLM Solutions AG (Lübeck, Germany). In addition, the effect of TiC nanoparticles on improving flowability is considered. The recoating performance is demonstrated with AlSi10Mg powders blended in-house with 6 µm boron carbide (B4C) particles. The addition of up to 30 vol% 6 µm B4C particles is investigated. The recoatability is described based on powder layer images which are analyzed for defects. High-speed images were recorded and evaluated to understand the mechanisms of the new recoating process. The properties of the powder feedstock are characterized differently (static/dynamic angle of repose and Hausner-Ratio) to search for a direct value that correlates with the recoatability.

2. Materials and methods

2.1. Materials

Aluminum powder from m4p material Solutions GmbH (Magdeburg, Germany) was used for the experiments. The bore carbide ceramic particles were supplied from Industriekeramik Hochrhein GmbH (Wutöschingen, Germany). The TiC-nanoparticles with an average diameter of 50 nm were bought from IoLiTec Ionic Liquids Technologies GmbH (Heilbronn, Germany). The chemical composition of the powder materials was measured through X-ray fluorescence (XRF) and optical emission spectrometry with inductively coupled plasma (ICP-OES) by the suppliers, Table 1. The particle morphology of the aluminum is potato-like and the B4C has a blocky shape. The delivered TiC-nanoparticles are clustered to agglomerates with a size between ~5 and 40 µm, measured in scanning electron microscopy (SEM) images. An overview of the particle morphology and the particle size distribution measured by dry laser diffraction using a Cilas 1090 is given in Fig. 1.

2.2. Calculation of TiC nanoparticle mass for percent surface coverage

The Surface Area Coverage (SAC) value indicates the percentage of the host particle surface that should be covered with guest particles in order to improve flowability. In order to calculate the required mass of guest particles for a given mass of host particles, various assumptions must be made. Fulchini et al. [29] postulate three assumptions for the calculation deviating from reality: First that all particles are ideal spheres and have a uniform diameter of their d_{50} value. Second that all guest particles adhere in a single layer on the host particle. Third the guest particles cover the surface of the host particles with the circular area of the guest particle diameter. For the calculation, the number of guest particles n_g is defined with the circular area $A_{\varnothing\_guest}$ required to cover SAC of a host particle sphere surface A_{S_host}, Eq. (1). Then the required mass of guest particles m_{guest} for a given mass of host particles m_{Al} is scaled (Eq. (4)) with the masses for one host m_{1_host} and guest m_{1_guest} particle, Eqs. (2), (3).

$$n_g = \frac{SAC \times A_{S\_host}}{A_{\varnothing\_guest}} = \frac{SAC \times \pi \times d_{50\_host}^2}{\pi/4 \times d_{50\_guest}^2} = \frac{4 \times SAC \times d_{50\_host}^2}{d_{50\_guest}^2} \quad \text{Number of needed guest particles for one host particle} \quad (1)$$

$$m_{1\_host} = \frac{1}{6} \times \pi \times d_{50\_host}^3 \times \rho_{host} \quad \text{Mass of one host particle} \quad (2)$$

$$m_{1\_guest} = \frac{1}{6} \times \pi \times d_{50\_guest}^3 \times \rho_{guest} \quad \text{Mass of one guest particle} \quad (3)$$

$$m_{guest} = \frac{n_g \times m_{1\_guest} \times m_{Al}}{m_{1\_host}} = \frac{4 \times SAC \times d_{50\_guest} \times \rho_{guest} \times m_{Al}}{d_{50\_host} \times \rho_{host}} \quad \text{Required mass of guest particles for a given mass of host particles} \quad (4)$$

In this work, AlSi10Mg and B4C were separately coated with a SAC of 25 %. Several other articles have shown that this value best increases flowability [29–31]. The calculation values and results of this investigation are given in Table 2.

2.3. Mixing and coating process

All MMC feedstocks were mixed in a round 2 l powder container from AMproved GmbH (Paderborn, Germany) using an in-house conceptualized two-axis 3D tumbling mixer. The powders to be mixed or coated are tumbled for 30 min. Picking four samples of 6 ml material with a self-designed sample picker at the bottom edge of the bottle proves that the mixing time of 30 min is sufficient. The feedstocks are homogeneous as

Table 1
Chemical composition of the AlSi10mg and B4C powder particles in wt%.

	Fe	Si	Mg	Mn	Ti	Zn	Cu	Pb	Sn	Ni	Al	Ca	B4C
AlSi10Mg	0.18	9.8	0.35	0.01	0.03	0.01	<0.01	<0.01	<0.01	<0.01	Base		
B4C	0.34	0.4			<0.01						0.04	0.04	Base

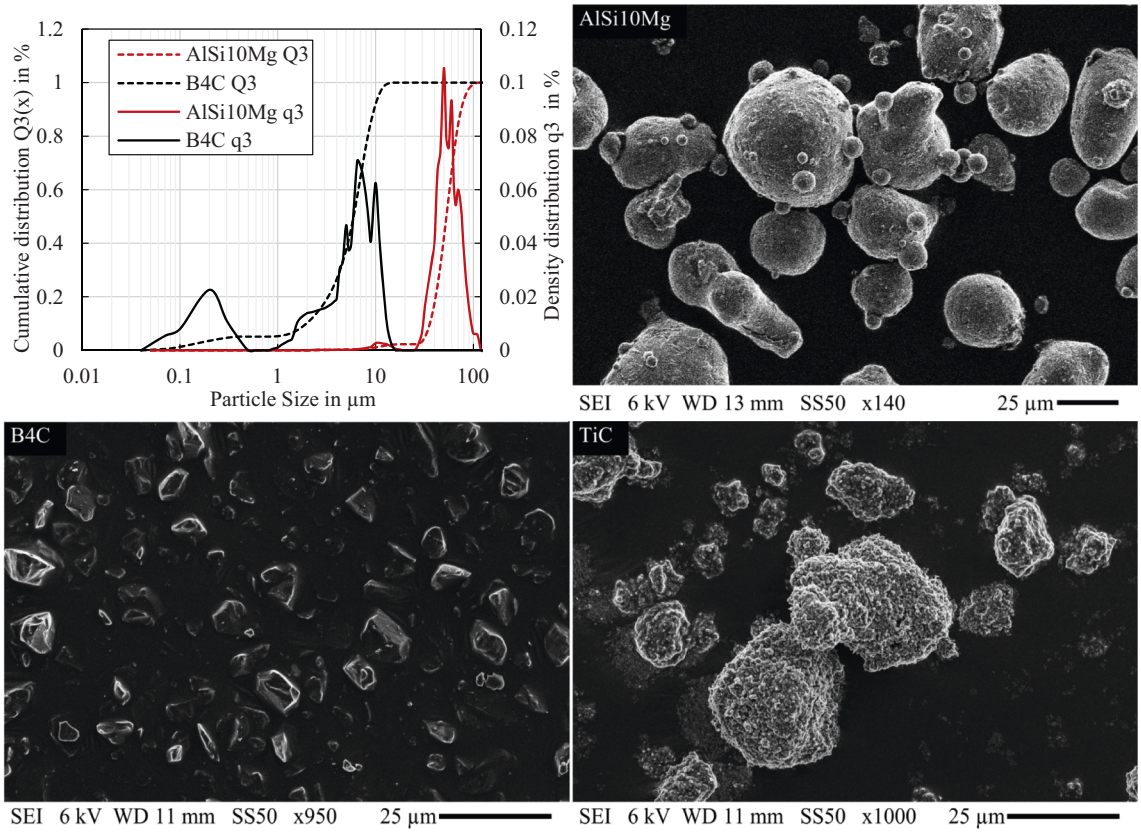

Fig. 1. Particle size distribution and SEM images of the Alsi10Mg, B4C, and TiC powders.

Table 2
Material density, median particle size, and wt% to cover with TiC-nanoparticles.

	Density in g/cm^3	d_{50} in µm	TiC in wt% for 25 % SAC
AlSi10Mg	2.67	43.51	0.23
B4C	2.59	5.67	1.67
TiC	4.93	0.05	

the particle size distribution analysis for a feedstock with 15 vol% B4C shows similar results, Table 3. Adding the smaller particles should theoretically decrease the d_{50} value compared to the measured value for pure AlSi10Mg. The increased value is attributed to the forming of agglomerations of AlSi10Mg and B4C particles.

Table 3
Comparison of four picked samples from a 15 vol% feedstock mixture after 30 min of mixing to prove the homogeneity and values for pure AlSi10Mg and B4C.

Sample nr.	d_{10} in µm	d_{50} in µm	d_{90} in µm
AlSi10Mg	29.52	43.51	60.17
B4C	1.95	5.95	9.67
1	8.73	47.64	71.63
2	8.57	47.59	73.16
3	8.52	47.9	72.76
4	8.87	47.8	72.22
Scatter in %	1.59	0.25	0.79

To coat AlSi10Mg or B4C with TiC nanoparticles, already TiC-coated 2 mm 1.4043 grinding balls were added to the mixing bottle to break up the large agglomerates of the original TiC-nanoparticle powder. The ball's weight was six times the mass of the powder to be coated. After the coating process, the powders were sieved through a Ø200 mm 63 µm analytical sieve using an AS 200 Control sieve tower from Retsch GmbH (Haan, Germany) with an acceleration of 1.15 g to remove the balls. The sieving process is accelerated by connecting a broadband converter from Telsonic AG (Bronschhofen, Switzerland). The coating results are presented in [31]. A volume of 500 ml was prepared for each feedstock.

2.4. Measurement of powder properties

In this study the Hausner-Ratio, static and dynamic angles of repose, describing the flowability of powders, were compared. The Hausner-Ratio is the tap and apparent density quotient [39]. The apparent density of the feedstocks was measured according to the ISO 3923-2 standard using a Scott Volumeter from 3P Instruments GmbH & Co. KG (Odelzhausen, Germany) and a 25 ml cup. To ensure a complete filling of the cup and to reduce the scatter of the experiments, 30 ml of material were added to the funnel of the Scott volumeter at a time. The powder pile on the cup was removed by pushing a blade at a 45° angle twice in two directions. The weight was then determined using an XSR204 precision balance from Mettler Toledo GmbH (Greifensee, Switzerland). The tap density was measured according to the ISO 3953 standard using

a BeDensi tap machine from 3P Instruments GmbH & Co. KG (Odelzhausen, Germany). A 100 ml measuring cylinder was filled with 100 ± 0.1 g powder for the experiments. The test was run with a tap frequency of 200 Hz for 3000 taps to ensure no further powder compaction occurred.

Besides the Hausner-Ratio, the static or dynamic angle of repose can be measured. The static angle of repose was measured according to the ISO 4324 standard. The dynamic angle of repose was recorded using a revolution powder analyzer from Mercury Scientific Inc. Due to the poor flowability of the feedstocks, both values could not be measured. The static angle could not be measured as only rugged piles formed, Fig. 2a. The dynamic angle could not be measured because the feedstocks stuck to the drum wall, Fig. 2b. This effects also occurred when measuring feedstocks with nanoparticle coating. The significant improvement in flowability observed by Fulchini et al. [29] and Gärner et al. [30] due to nanoparticle coating, which allowed them to measure the static or dynamic angle of repose, was not achieved for the AlSi10Mg + B4C feedstocks. These results show that the static and dynamic angles of repose are unsuitable for describing highly cohesive PAMC powders and will not be further discussed in this article.

2.5. Machine adaption for ultrasonic recoating

Modifying the recoating system of industrial PBF-LB machines is difficult due to the compact construction. Further, machines with a powder tank require approximately 1 l of powder material to produce 10 mm high specimens, even with a build chamber size of Ø100 mm. Neither of these aspects is suitable for investigating new material compositions and their recoating processes. Therefore, a new recoater carriage for a SLM280HL 1.0 from SLM Solutions AG (Lübeck, Germany) was developed. The carriage consists of a powder tank, a dosing slide, and the option to mount different recoating systems. The designed tank has a volume of 1.4 l, which allows the production of specimens with a height of 65 mm built on a build platform with a diameter of 100 mm. The dosing slide consists of an exchangeable metal sheet with a defined rectangular opening to deposit a defined powder volume. At the end of the recoater moving path, the opening of the metal sheet is pushed in opposite direction and releases the powder in front of the recoating system. When moving backward, the metal sheet is pushed back by springs. To mount different recoating systems or adjust the height, they are mounted to a rectangular block that can be moved up and down and fixed with two flat ball screws at any height, Fig. 3.

2.6. Ultrasonic system

For the experiments in this article, a broadband ultrasonic system was chosen. The system consists of a broadband converter and source, which can vary the supplied energy to the converter between 30 and 100 % from Telsonic AG (Bronschhofen, Switzerland). The source constantly varies the frequency between 35 and 37 kHz. As a result, a resonant frequency of the excited parts is always met, causing them to vibrate. This allows a freer design of the sonotrode compared to resonance-excited systems. For easy replacement of the actual coating geometry, which is in direct contact with the powder and therefore subject to wear, screw connections can be provided. Since rubber damps vibrations, no rubber lips were used as recoating geometry. Metal or ceramic blades are also rarely used in PBF-LB because they are expensive and also wear out. Consequently, cheap metal combs from electron beam machines were used. They are available as spare parts of an Arcam Electronic Beam machine from GE Additive (Norwalk, United States of America). At the bottom of the sonotrode, two pairs of metal combs are arranged at a distance of 2 mm from each other and clamped with flat ball screws to the sonotrode. Comb pairs are used to avoid stripes in the powder layer. The teeth of the second comb of a pair cover the gap between the teeth of the first. The combs are 0.1 mm thick and have a teeth height of 10 mm.

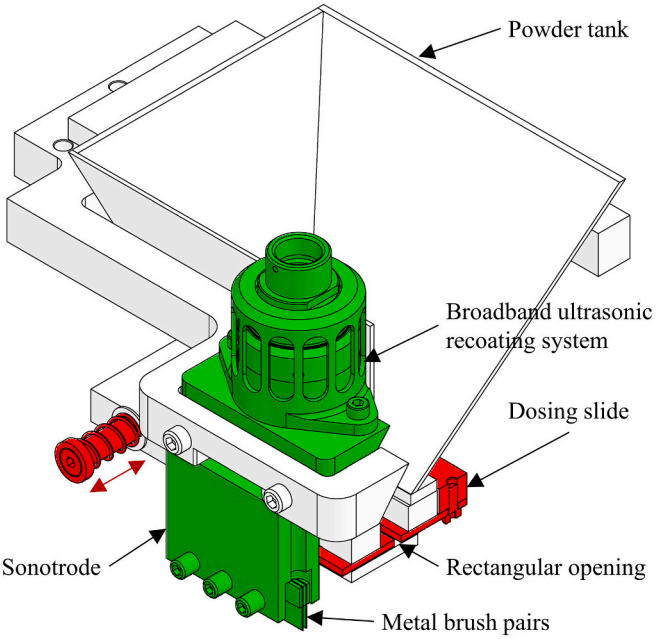

Fig. 3. Principal of a recoater carriage for a SLM280 HL 1.0 with its own tank and exchangeable recoating system.

Since the SLM 280 HL does not have an open control interface, an additional mechanical position switch was mounted on the recoating carriage to switch off the ultrasonic source as soon as the recoating carriage has moved and the laser exposure of the layer begins. Besides the high-voltage cable to the converter and the control cable for the switch, a grounding cable was connected to the converter to ensure the safe operation of the system even in the event of a malfunction of the ultrasonic system.

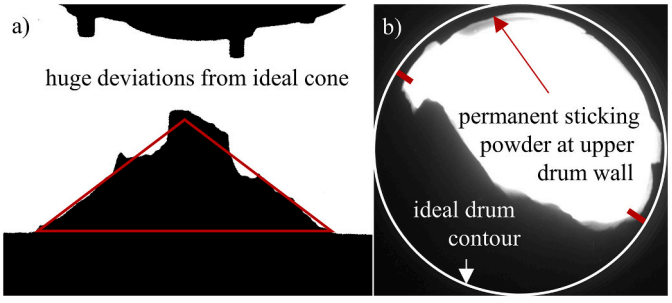

Fig. 2. Issues measuring the static a) and dynamic b) angle of repose of AlSi10Mg + 20 vol% B4C.

2.7. Recoating experiments and highspeed camera observation

For the recoating experiments in the SLM280HL, a metal sheet with a dosing volume of 0.69 ml was mounted to the dosing slide, and an EN AW5083 building platform was mounted in the build chamber. To simulate the roughness of an AlSi10Mg powder layer or the as-build surface without remelting, the platform was glass bead blasted. The S_a and S_z values of all conditions were three times measured at different locations with a confocal microscope from Nanofocus AG (Karlsruhe, Germany), Table 4. As the roughness of the blasted platform is still lower than the as-build or powder roughness, the form fit is insufficient to coat a usual layer thickness of 50 µm with pure AlSi10Mg powder without defects. For this reason, the layer thickness of the recoating experiments was increased to 209 µm until pure AlSi10Mg could be recoated without defects. The results of these investigations are nevertheless valid for 50

Table 4
Deviation of the surface roughness of the building platform in the recoating experiments compared to the real surface roughness of the powder bed in the process and the as-build part surface measured with a confocal microscope.

	S_a in µm	S_z in µm
Glass bead blasted EN AW5083	3.15 ± 0.04	42.93 ± 1.31
Recoated AlSi10Mg powder	23.53 ± 0.48	219.33 ± 9.46
As build AlSi10Mg without remelting	15.85 ± 2.25	168 ± 31.21

µm layers, too. In subsequent investigations in which the component build-up was examined, an initial 50 µm coating with ultrasonic excitation was possible and the build-up process was stable. In the first three layers, the quality is not always flawless, but from the fourth layer onwards, the quality corresponds to the following presented results. This is usually unproblematic because support structures are mostly provided under components, and the first layers are lost when the components are cut off the building platform.

In order to evaluate the quality of the powder layers, an optical analysis was developed. A minimum of five layers were recoated and captured with a DSLM camera G91 from Panasonic, which was additionally mounted to the recoater carriage. After each recorded layer, the deposited powder was entirely removed. A led ring light KR90 from Kaiser Fototechnik GmbH& Co. KG (Buchen, Germany) with a color temperature of 5500 K and an illuminance of approx. 2100 lx was mounted on the camera's lens to capture shadow-free images of the layers. The recorded images had a resolution of 5184 × 3888 px^2 or 77.76 × 58.32 mm^2, corresponding to a 15 µm/pixel resolution. The images represent the center of the Ø100 mm building platform. Defects in the powder layers, areas without powder deposition, were automatically marked with a Matlab code. Firstly, the code converted the image into a gray image. The contrast was then enhanced using the Matlab function *adapthisteq*. The additive binarization of the image could not sufficiently separate the background (light gray/red label) of the images from the powder (dark gray), which is why a fixed threshold was set as shown in Fig. 4. The percentage of marked defect pixels to the total number is then evaluated and is further called the surface proportion of defects and is the response variable of this investigation. An overview of all factor settings of the partial factorial experimental design is shown in Table 5. The integration of the ultrasonic system and the experimental setup for analyzing the layer quality are shown in Fig. 5a.

To understand the mechanisms of the broadband ultrasonic recoating process, high-speed camera videos were recorded to analyze the metal comb vibration and the powder flow in detail. The recoating system was mounted to a CMX 70 mill machine spindle from DMG Mori K.K. A.G. (Nagoya, Japan) to improve the visible access to the system, Fig. 5b. The metal comb movement was recorded with 16 k frames/s and 120 k frames/s and analyzed with the free software tracker from physlets. As the highspeed setup deviated from the SLM system did not have a powder tank, the powder was deposited in front of the metal combs with a 5 ml dosing spoon to observe the powder flow. Further, the milling machine moved the building platform underneath, and the ultrasonic system was held in position, deviating from the powder bed process.

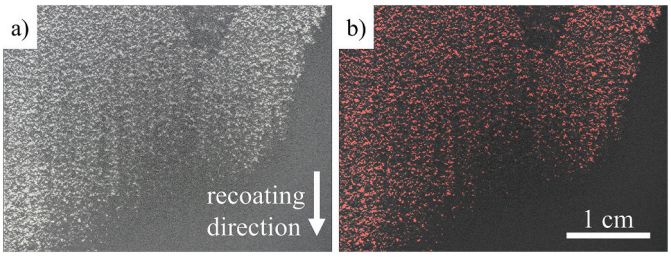

Fig. 4. a) Photo after recoating b) labeling of the coating defects by the Matlab code. The analysis shows a defectively recoated area of 6.56 %.

Table 5
Overview of all factors and the according level values of the partial factorial experimental design that were investigated in 65 different test points.

Feedstocks	TiC-coating	Recoating speeds	Ultrasonic intensity
AlSi10Mg	0	52.5 mm/s	30 %
+10 vol% B4C	25 SAC	70 mm/s	50 %
+15 vol% B4C		87.5 mm/s	70 %
+20 vol% B4C			90 %
+25 vol% B4C			100 %
+30 vol% B4C			

However, this deviation allows the powder movement to be observed continuously. The powder flow during recoating was recorded with 50 k frames/s.

3. Results

3.1. High-speed analysis of metal combs movement

The recordings with different frame rates show that every metal comb vibrates with two superimposed modes. The first mode oscillates sinusoidal in and against the recoating direction, Fig. 6b. The second mode shows a superimposed smaller movement with the highest frequency and amplitude at the switching points of the direction of motion, Fig. 6c.

Analyzing the motion shows that the first mode's movement frequency remains constant for all intensities. Increasing the ultrasonic intensity from 30 % to 50 % increases the amplitude of the first mode. A further increase in intensity does not affect the amplitude. The continuously changing frequency by the source causes the high spread in the amplitude of the first mode, Fig. 7a. The frequency of the second mode rises strongly from 30 % to 50 %. The amplitude continuously increases slightly with increasing intensity, Fig. 7b. The high velocity of motion at intensities above 30 % increases the second mode scatter, Fig. 7b. The recording frequency is no longer twice as high as the motion velocity all the time, which violates the Nyquist-Shannon sampling theorem [40]. At an intensity of 90 %, the movement is so low resolved that an analysis is no longer possible.

At intensities higher than 50 %, the system seems to saturate. Theoretically, the amplitude of the first mode should continually increase if the frequency is constant and the intensity increase. It is assumed that the higher intensities lead to an amplification of the bending modes within the combs, which causes them to wriggle more strongly increasing the second mode amplitude. The calculation of the energy of the second mode supports this assumption. There is a linear increase in energy with increasing intensity, Fig. 8.

3.2. Influence of ultrasonic metal comp excitation and nanoparticle coating on the powder layer quality

No defects are allowed in the powder layer to be suitable for the PBF-LB process. Without ultrasonic excitation exclusively AlSi10Mg have 0 % surface proportion of defects. Up to an addition of 15 vol% B4C, the percentage of defects increases moderately. Smaller round spots form at the recordings' edge where the material is insufficiently deposited. These defects are similar to the one in Fig. 4 but less. From an addition of 20 vol%, almost no powder is deposited. Individual wavelike powder lines and homogeneously distributed small powder dots are formed. Besides, a clear correlation with the recoating speed is observed at 10 and 15 vol% B4C. The recoating defect decreases with decreasing recoating velocity. The influence is no longer apparent at the higher B4C volume fractions due to the generally insufficient layer deposition, Fig. 9.

Ultrasonic excitation at 50 % intensity significantly reduces the number of coating defects even at higher vol% B4C. Reducing the recoating velocity, reduces the defect percentage further like without

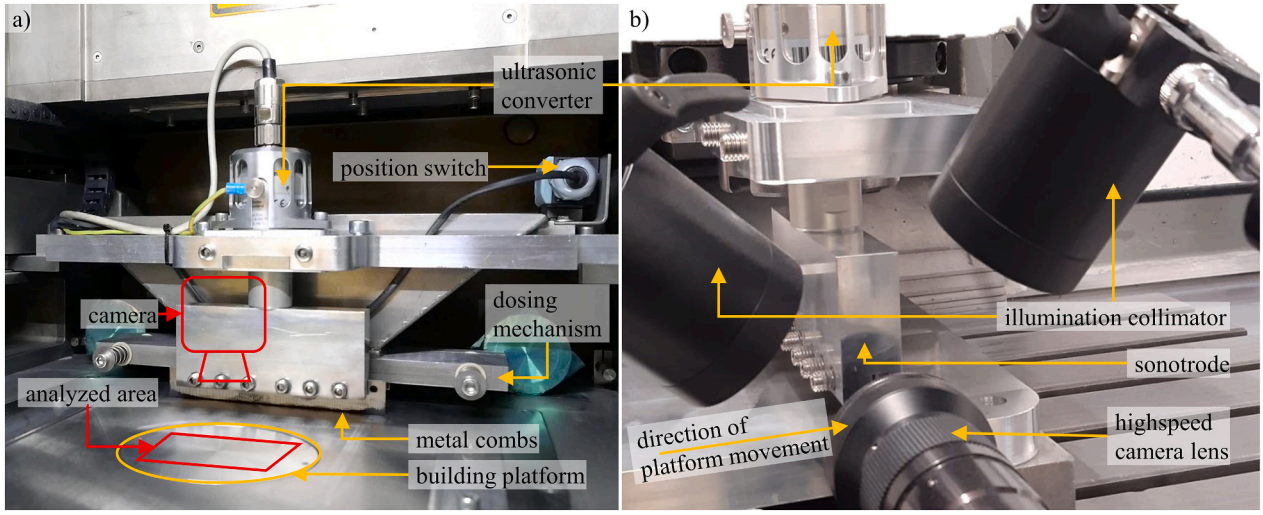

Fig. 5. a) machine adoption, ultrasonic excitation integration, and layer quality observation setup b) Highspeed camera setup in CMX mill machine to observe metal comb movement and powder flow in detail.

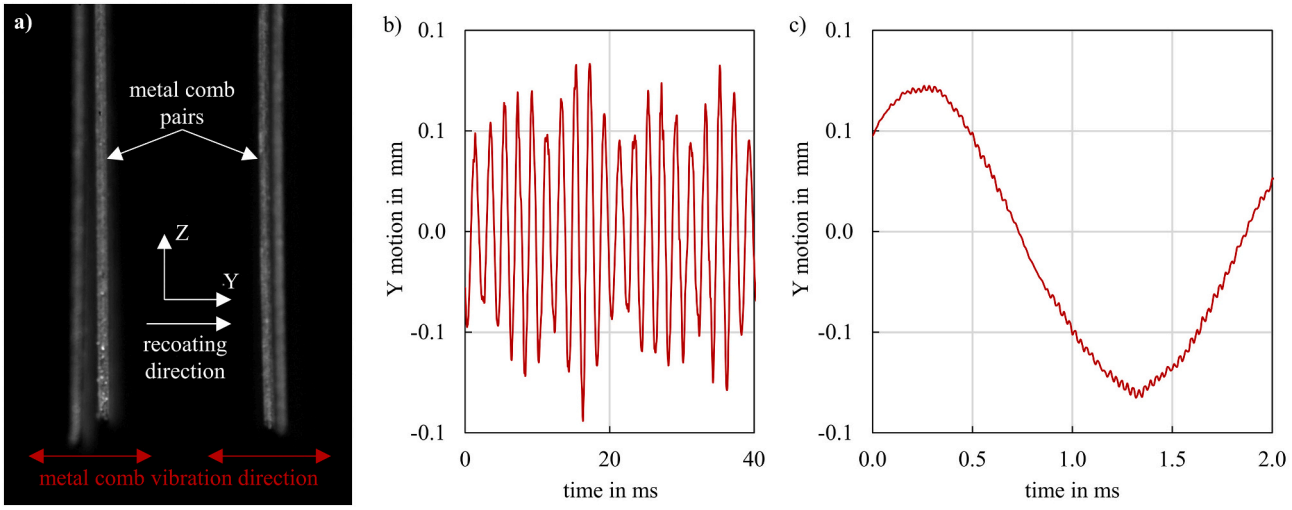

Fig. 6. a) High-speed camera image for analyzing the metal comb movement, b) Evaluation of the movement at 16 k fps resolution showing the first mode, c) 120 k fps resolution showing the second mode.

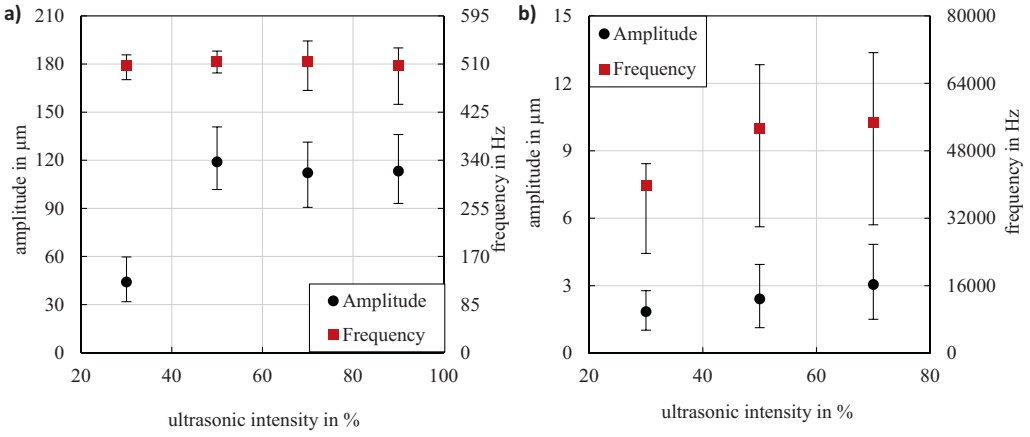

Fig. 7. Analyzed amplitude and frequency of the metal comb of a) the first mode, b) the second mode.

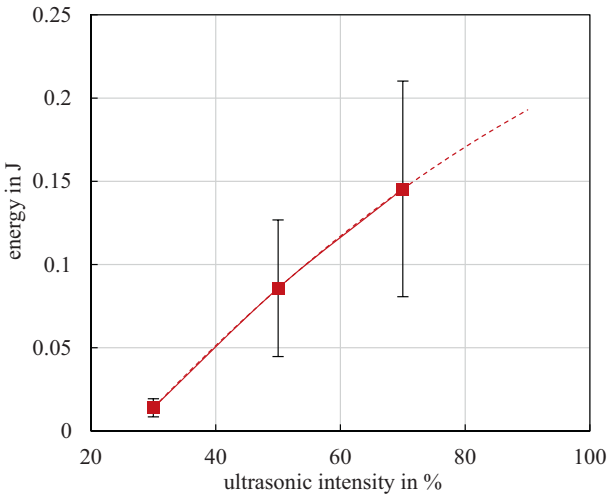

Fig. 8. Calculated energy of the second mode of the ultrasonic excitation.

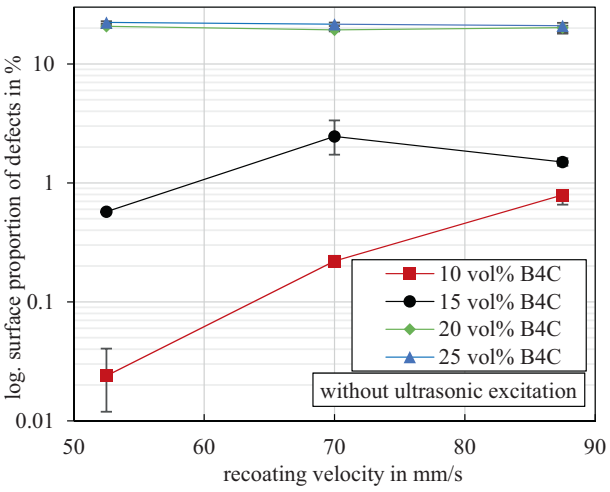

Fig. 9. Influence of recoating velocity and B4C volume fraction on surface proportion of defects without ultrasonic excitation.

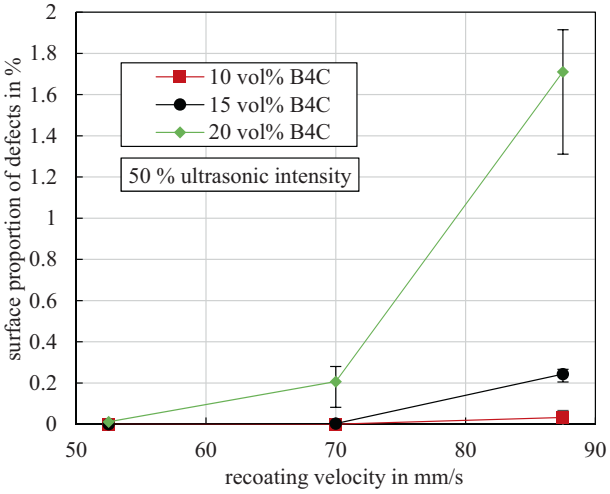

Fig. 10. Influence of recoating velocity and B4C volume fraction on the surface proportion of defects with 50 % intense ultrasonic excitation.

ultrasonic excitation, Fig. 9, so even feedstocks with 20 vol% B4C can be recoated without defects, Fig. 10.

The nanoparticle coating also significantly decreases the recoating defects. This effect is observed for the recoating without and with ultrasonic excitation at different intensities. However, coating with nanoparticles alone is insufficient to achieve defect-free layers, Fig. 11. In summary, the process map for the broadband ultrasonically excited process is as indicated in, Fig. 11. This map shows the process limits of the current setup. Feedstocks with 30 vol% B4C can no longer be entirely coated without defects, even with nanoparticle coating.

3.3. Influence of vol% B4C and nanoparticle coating on the Hausner-Ratio

The Hausner-Ratio value shows a continuous increase with increasing vol% B4C. However, from a content of 15 vol%, the Hausner-Ratio increases more strongly. Up to this gradient change, the Hausner-Ratio can be calculated as the percentage of the Hausner-Ratio of pure AlSi10Mg and pure B4C with a Hausner-Ratio of 2.25 ± 0.0018. The value of the Hausner-Ratio at 15 vol% is nearly at the boundary between passable and cohesive flowability [39], Fig. 12. The comparison of the recoating tests without ultrasonic excitation, Fig. 9, seems to show a correlation, as the materials with nearly very cohesive (20 vol% B4C) or very cohesive (from 25 vol% B4C) properties, according to Hausner, were also not recoatable. The effect of the nanoparticle coating is also reflected in the measurement of the Hausner-Ratio. The value for 20 vol % B4C + 25 % SAC TiC decreases strongly and is only 0.005 higher than the measured value for 15 vol% B4C, Fig. 12. However, comparing the coating defects without ultrasonic excitation shows a significant difference of 13 % between 15 vol% B4C without nanoparticle coating and 20 vol% B4C + 25 % SAC TiC, Fig. 11, which rules out a direct relationship between the Hausner-Ratio and recoatability.

4. Discussion

4.1. Recoating process

The results show that the ultrasonic excitation allows the recoating of non-flowable feedstocks. This means that the energy transferred to the feedstocks by the vibrating metal combs affects the two mechanisms that decrease flowability: internal powder friction and agglomeration. The recorded high-speed images show that the fast movement of the metal combs gives an impulse to the particles in direct contact over the

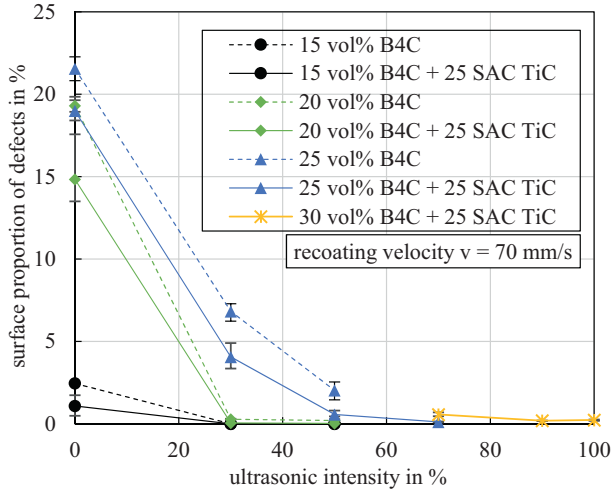

Fig. 11. Overview of the coating test results. Illustration of the ultrasonic intensity required for a certain vol% of B4C and whether additional nanoparticles need to be added in order to coat defect-free layers.

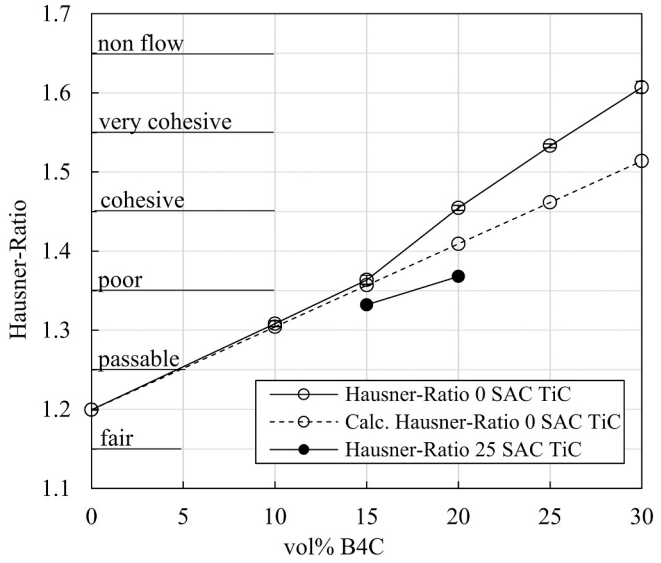

Fig. 12. Powder feedstock Hausner-Ratio change depending on the volume percent B4C. Left axis: Flow properties according to Hausner-Ratio.

complete comb height. The applied impulse force accelerates the particles in the recoating direction. The images indicate that the compacted powder pile is held in position through the friction force between the platform and the powder pile. The impulses at the tip of the comb shear off the powder pile, whereby large agglomerates are torn apart into single AlSi10Mg particles with adhered B4C particle satellites. It is deduced that the energy introduced by the impulses is large enough to overcome the Van der Waals, electrostatic, and friction forces in the powder pile, making the recoating possible, Fig. 13b. Without ultrasonic excitation, the inner forces of the powder pile are higher than the friction force between the building platform and the powder pile. Hence, no recoating is possible, Fig. 13a. Furthermore, during ultrasonic excitation, the powder pile is set in rotation in front of the metal comb, Fig. 13b. This effect was also simulated by Phua et al. [41] and resulted in the simulation in a smoother powder bed. However, powder rotation does not occur when recoating without ultrasonic excitation.

The evaluation of the high-speed recordings further shows that the energy is mainly transferred by the second mode oscillation since the first mode motion is mostly hindered by the powder pile in front of it. The increasing energy, Fig. 8, results in a higher impulse force, allowing material with higher internal forces (in this case, higher vol% B4C) to be sheared off and recoated.

According to the results of Gärtner et al. [24,30], the higher distance of the particles to each other, if they are coated with nanoparticles, the Van der Waals and electrostatic forces, as well as the friction, are reduced, leading to a decrease of the surface proportion of defects. In addition, the reduced forces make it easier to shear the feedstocks with coated particles, explaining the decreasing surface proportion of defects when recoating them with ultrasonic excitation, Fig. 11.

The ultrasonic excitation described in this article differs from the other approaches simulated by Schiochet et al. [38] or experimentally investigated by Drechsel et al. [42]. While vertical excitation was investigated in the mentioned studies, this study used horizontal excitation. All approaches resulted in a better coating quality or allowed the coating of agglomerating powders. However, it is assumed that horizontal excitation is more beneficial because the deflection of the recoating geometry caused by the excitation cannot lead to collisions with material that has already been built up. As a result, the coating quality should be consistent during the building process, and wear on the recoating geometry should be less.

4.2. *Description of recoat ability by powder properties*

The measurement of the Hausner-Ratio provides contradictory results related to the recoatability and cannot describe the dependence on the recoating velocity. Further classical methods for determining flowability are unsuitable for describing the recoatability of strongly agglomerating PAMCs feedstocks. Contrary to the results of other publications that have worked with a higher proportion of fines of the same material and morphology in their investigations and were able to determine the static and dynamic angle of repose [24,29,30], this was not possible for the PAMCs investigated here, see Fig. 2. For this reason, more elaborate coating tests must be carried out compared to flow tests.

5. Conclusion and outlook

This article presented a new approach for recoating non-flowing agglomerating powder feedstocks. To effectively study the recoating and processing of these feedstocks, a recoater carriage with its own tank was developed to reduce the amount of powder required for the experiments compared to the standard setup of an SLM280HL machine. To be able to coat the non-agglomerating powders, a broadband, ultrasonically excited recoater brush was developed. The horizontal vibration transfers energy to the powder and overcomes the adhesion forces

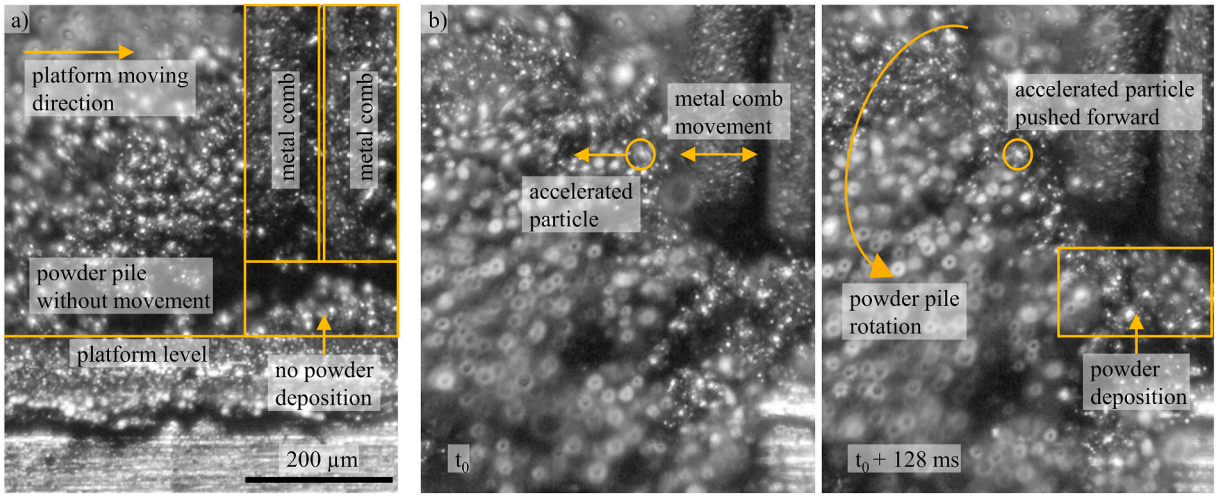

Fig. 13. Images of the highspeed recordings of the recoating process of AlSi10Mg + 20 vol% B4C a) without ultrasonic excitation, b) with ultrasonic excitation. Please watch the video in the appendix to fully identify the differences in the recoating with and without ultrasonic excitation.

in the powder by shear pulses so that the powder can be applied evenly.

Image analysis was used to determine the recoating quality, which detects non-recoated areas and interprets them as a percentage error to the total area. The investigation of the recoatability of strongly agglomerating feedstocks can currently only be carried out using this method. The use of alternative parameters describing the flowability did not provide a connection. The static and dynamic angle of repose and the Hausner-Ratio were tested.

Besides the influence of ultrasonic excitation on recoating, the flowability improvement by nanoparticles was also investigated. It was shown that both approaches can be used together. Thus, it is possible to recoat AlSi10Mg feedstocks with up to 25 vol% d_{50} 6 µm B4C particles without defects. These results now enable to investigate the production of B4C ceramic composite components with aluminum matrix in PBF-LB.

A brief trial with a −0/63 µm 1.4404 feedstock, which was also agglomerating and cannot be recoated with available technology because the fines were not removed after atomization, could also be recoated with ultrasonic excitation without any defects. This result demonstrates that the newly developed recoating technology works for the feedstocks discussed in detail in this article and generally has the potential to recoat agglomerating powders.

CRediT authorship contribution statement

Victor Lubkowitz: Writing – original draft, Visualization, Project administration, Methodology, Investigation, Formal analysis, Data curation, Conceptualization, Validation. **Kai Drechsel:** Writing – review & editing, Conceptualization. **Volker Schulze:** Writing – review & editing, Supervision, Resources, Funding acquisition. **Frederik Zanger:** Writing – review & editing, Supervision, Resources.

Declaration of competing interest

The authors declare that they have no known competing financial interests or personal relationships that could have appeared to influence the work reported in this paper.

Data availability

Data will be made available on request.

Acknowledgement

This Project is supported by the Federal Ministry for Economic Affairs and Climate Action (BMWK) based on a decision by the German Bundestag.

Appendix A. Supplementary data

Supplementary data to this article can be found online at https://doi.org/10.1016/j.jmapro.2024.07.118.

References

[1] Bendsøe MP, Sigmund O. Topology optimization: Theory, methods, and applications. 2nd ed. Berlin, Heidelberg: Springer; 2004.
[2] Poorganji B, Ott E, Kelkar R, Wessman A, Jamshidinia M. Review: Materials ecosystem for additive manufacturing powder bed fusion processes. JOM 2020;72(1):561–76.
[3] Stopyra W, Gruber K, Smolina I, Kurzynowski T, Kuźnicka B. Laser powder bed fusion of AA7075 alloy: Influence of process parameters on porosity and hot cracking. Addit Manuf 2020;35:101270.
[4] Ludwig Ina. Increasing resource efficiency of aviation by innovative materials and bionic design for metal components made by additive manufacturing. https://www.aerospace3dprintingconference.com/wp-content/uploads/2021/06/20210608_A3DP-Conference_IAPT_Ina-Ludwig_compressed.pdf.
[5] Jia Q, Rometsch P, Cao S, Zhang K, Wu X. Towards a high strength aluminium alloy development methodology for selective laser melting. Mater Des 2019;174:107775.
[6] Spierings AB, Dawson K, Dumitraschkewitz P, Pogatscher S, Wegener K. Microstructure characterization of SLM-processed Al-Mg-Sc-Zr alloy in the heat treated and HIPed condition. Addit Manuf 2018;20(0):173–81.
[7] Yu W, Xiao Z, Zhang X, Sun Y, Xue P, Tan S, et al. Processing and characterization of crack-free 7075 aluminum alloys with elemental Zr modification by laser powder bed fusion. Mater Sci Add Manuf 2022;1(1):4.
[8] Chawla N, Jones JW, Andres C, Allison JE. Effect of SiC volume fraction and particle size on the fatigue resistance of a 2080 Al/SiC p composite. Metall Mater Trans A 1998;29(11):2843–54.
[9] Haferkamp L, Haudenschild L, Spierings A, Wegener K, Riener K, Ziegelmeier S, et al. The influence of particle shape, powder flowability, and powder layer density on part density in laser powder bed fusion. Metals 2021;11(3):418.
[10] Zhao Y, Cui Y, Hasebe Y, Bian H, Yamanaka K, Aoyagi K, et al. Controlling factors determining flowability of powders for additive manufacturing: a combined experimental and simulation study. Powder Technol 2021;393:482–93.
[11] Takahashi T, Kinai Y, Osada T, Kobayashi S. Effect of water atomized powder size on the flowability and sintered properties in metal binder jet 3D printing. Mech Eng J 2023;10(4) [22-00476-22-00476].
[12] Thalberg K, Lindholm D, Axelsson A. Comparison of different flowability tests for powders for inhalation. Powder Technol 2004;146(3):206–13.
[13] Krantz M, Zhang H, Zhu J. Characterization of powder flow: Static and dynamic testing. Powder Technol 2009;194(3):239–45.
[14] Schatt W, Wieters K-P, Kieback B. Pulvermetallurgie. Berlin Heidelberg: Springer; 2007.
[15] Gu D, Chang F, Dai D. Selective laser melting additive manufacturing of novel aluminum based composites with multiple reinforcing phases. J Manuf Sci Eng 2015;137(2):21009.
[16] Xue G, Ke L, Liao H, Chen C, Zhu H. Effect of SiC particle size on densification behavior and mechanical properties of SiCp/AlSi10Mg composites fabricated by laser powder bed fusion. J Alloys Compd 2020;845:156260.
[17] Zhao X, Gu D, Ma C, Xi L, Zhang H. Microstructure characteristics and its formation mechanism of selective laser melting SiC reinforced Al-based composites. Vacuum 2019;160(3):189–96.
[18] Haeri S. Optimisation of blade type spreaders for powder bed preparation in additive manufacturing using DEM simulations. Powder Technol 2017;321:94–104.
[19] Fucito K. Influence of blade gap thickness and recoater velocity on powder layer quality in additive manufacturing. Auburn; 2020.
[20] Yuasa K, Tagami M, Yonehara M, Ikeshoji T-T, Takeshita K, Aoki H, et al. Influences of powder characteristics and recoating conditions on surface morphology of powder bed in metal additive manufacturing. Int J Adv Manuf Technol 2021;115(11−12):3919–32.
[21] Shen M-Y, Tian X-J, Liu D, Tang H-B, Cheng X. Microstructure and fracture behavior of TiC particles reinforced Inconel 625 composites prepared by laser additive manufacturing. J Alloys Compd 2018;734:188–95.
[22] Cappella B, Dietler G. Force-distance curves by atomic force microscopy. Surf Sci Rep 1999;34(1–3):1–104.
[23] Karg MCH, Munk A, Ahuja B, Backer MV, Schmitt JP, Stengel C, et al. Expanding particle size distribution and morphology of aluminium-silicon powders for Laser Beam Melting by dry coating with silica nanoparticles. J Mater Process Technol 2019;264:155–71.
[24] Gärtner E, Jung HY, Peter NJ, Dehm G, Jägle EA, Uhlenwinkel V, et al. Reducing cohesion of metal powders for additive manufacturing by nanoparticle dry-coating. Powder Technol 2021;379:585–95.
[25] Lüddecke A, Pannitz O, Zetzener H, Sehrt JT, Kwade A. Powder properties and flowability measurements of tailored nanocomposites for powder bed fusion applications. Mater Des 2021;202(1–2):109536.
[26] Hartmüller J, Ripperger S. Berechnung der Haftung von Pulverpartikeln an strukturierten Oberflächen. Chem Ing Tech 2014;86(8):1260–8.
[27] Dutta B. Science, technology and applications of metals in additive manufacturing. San Diego: Elsevier; 2019.
[28] Barthel H, Rösch L, Weis J. Fumed Silica - production, properties, and applications. In: Auner N, Weis J, editors. Organosilicon Chemistry Set. Wiley; 2005. p. 761–78.
[29] Fulchini F, Zafar U, Hare C, Ghadiri M, Tantawy H, Ahmadian H, et al. Relationship between surface area coverage of flow-aids and flowability of cohesive particles. Powder Technol 2017;322:417–27.
[30] Gärtner E, Uhlenwinkel V. Nanosized additives enhancing metal powder flowability in additive manufacturing applications. In: AWT-Fachkonferenz, Werkstoffe – Prozesse – Wärmebehandlung; 2022. p. 12–20.
[31] Lubkowitz V, Scherer T, Schulze V, Zanger F. Influence of TiC-nanoparticles on the material properties of AlSi10Mg manufactured by laser powder bed fusion. In: Solid free form conference; 2023.
[32] Chianrabutra S, Mellor BG, Yang S. A dry powder material delivery device for multiple material additive manufacturing. Solid free form conference. 2014.
[33] Wei C, Gu H, Sun Z, Cheng D, Chueh Y-h, Zhang X, et al. Ultrasonic material dispensing-based selective laser melting for 3D printing of metallic components and the effect of powder compression. Addit Manuf 2019;29(1):100818.
[34] Wei C, Gu H, Zhang X, Chueh Y-h, Li L. Hybrid ultrasonic and mini-motor vibration-induced irregularly shaped powder delivery for multiple materials additive manufacturing. Addit Manuf 2020;33:101138.
[35] Kollmann T, Tomas J. Effect of applied vibration on silo hopper design. Part Sci Technol 2002;20(1):15–31.

[36] Teidelt E, Starcevic J, Popov VL. Influence of ultrasonic oscillation on static and sliding friction. Tribol Lett 2012;48(1):51–62.
[37] Dunst P, Bornmann P, Hemsel T, Sextro W. Vibration-assisted handling of dry fine powders. Actuators 2018;7(2):18.
[38] Schiochet Nasato D, Briesen H, Pöschel T. Influence of vibrating recoating mechanism for the deposition of powders in additive manufacturing: discrete element simulations of polyamide 12. Addit Manuf 2021;48:102248.
[39] Hausner HH, Mal MK. Handbook of powder metallurgy. 2nd ed. New York, N.Y: Chemical Publ. Co; 1982.
[40] Shannon CE. Communication in the presence of noise. Proc IRE 1949;37(1):10–21.
[41] Phua A, Doblin C, Owen P, Davies CHJ, Delaney GW. The effect of recoater geometry and speed on granular convection and size segregation in powder bed fusion. Powder Technol 2021;394(3):632–44.
[42] Drechsel K, Lubkowitz V, Albrecht L, Schäfer P, Schneider M, Schulze V, et al. Development of an ultrasonically excited recoating process in laser powder bed fusion to process non-spreadable 316L powder. Powder Technol 2024;432(4):119153.

Victor Lubkowitz graduated from the UAS Stralsund with a bachelor's and from Coburg with a master's degree in mechenical engineering. After graduation, he started working at wbk - Institute of Production Science in the research group of Prof. Dr.-Ing. habil. Volker Schulze and Prof. Dr.-Ing. Frederik Zanger. For his doctoral thesis under supervision of Prof. Dr.-Ing. habil. Volker Schulze, he focuses on metal-matrix composites. Thereby fine B4C particles are mixed with an aluminum powder to a non flowable feedstock which is processed in a laser powder bed fusion process to increase the mechanical properties of the new material.

Kai Drechsel is a graduate at Karlsruhe Institute of Technology and received both his bachelor's and his master's degree in mechanical engineering at KIT. After graduating, he began working at the wbk - Institute of Production Science in the research group of Prof. Dr.-Ing. habil. Volker Schulze and Prof. Dr.-Ing. Frederik Zanger. For his doctoral thesis he focues on the experimental and simulativ development of an ultrasonically excited recoating process in laser powder bed fusion and the processing of fine, agglomerating 316 L powder under the supervison of Prof. Dr.-Ing. habil. Volker Schulze.

Volker Schulze studied Mechanical Engineering at University Karlsruhe (TH). He received his PHD there in materials technology and worked as Postdoc on mechanical surface and heat treatments. Since 2008 he is one of the directors of wbk Institute of Production Science and also one of the directors of the Institute of Applied Materials at Karlsruhe Institute of Technology. His fields of interests are now mainly manufacturing technologies like cutting and additive manufacturing processes.

Frederik Zanger is an experienced manufacturing engineer in additive manufacturing, machining of metals, simulation of manufacturing processes, and digitalization of process chains. He has established the research group Additive Manufacturing at wbk Institute of Production Science at Karlsruhe Institute of Technology (KIT). As one of the directors of the institute, he holds the chair for digitalization of process development for additive manufacturing since 07/2023. His expertise in additive manufacturing is on powder bed fusion (metals), directed energy deposition (metals), binder jetting (metals) and vat photopolymerization (ceramics) processes.